

Bleeding alert map (BAM): The identification method of the bleeding source in real organs using datasets made on mimicking organs

Maina Sogabe ^{a,1}, Kaoru Ishikawa ^{a,1}, Toshihiro Takamatsu ^b, Koh Takeuchi ^c, Takahiro Kanno ^d, Koji Fujimoto ^e, Tetsuro Miyazaki ^a, Toshihiro Kawase ^f, Toshihiko Sato ^g, Kenji Kawashima ^{a,*}

^a The Department of Information Physics and Computing, The University of Tokyo, Japan

^b The department of Exploratory Oncology Research & Clinical Trial Center, National Cancer Center and Research Institute for Biomedical Sciences, Tokyo University of Science, Japan

^c Graduate School of Informatics, Kyoto University, Japan

^d Riverfield Inc., Japan

^e Real World Data Research and Development, Graduate School of Medicine, Kyoto University, Japan

^f Department of Information and Communication Engineering, School of Engineering, Tokyo Denki University, Tokyo, Japan

^g The Department of medicine, Fukuoka University, Japan

ARTICLE INFO

Keywords:

Bleeding source estimation

Endoscopic surgery

Pix2Pix

Training data from mimicking organs

ABSTRACT

In thoraco-laparoscopic surgery, the identification of a bleeding source is recognized as one of the most important issues with hemostasis during operation. However, previously proposed techniques are only capable of detecting an approximate bleeding region, not the precise location itself. To develop a system which can accurately localize a bleeding source, post-bleeding images and their corresponding bleeding source information may be required. However, to pinpoint bleeding sources from actual thoraco-laparoscopic surgery images is no easy task even for an experienced surgeon. In previous studies, a surgeon could only provide rectangular region information around a bleeding source. To address the problem, we have developed a mimicking device that simulates bleeding from a vessel on an artificial organ for obtaining bleeding images and precise bleeding source information at the same time. Using this information, we constructed a Generator that can associate a bleeding image with the corresponding bleeding source by using Pix2Pix and created a “bleeding alert map (BAM)” which concerns the Predicted intensity of bleeding source in the endoscopic view. The Generator successfully created BAMs from ex vivo lung bleeding images as well as actual organ bleeding images captured in thoracoscopic surgeries. The results showed that the BAM Generator constructed only by using the data from the mimicking device was effective in processing bleeding images from actual organs to identify bleeding sources. The proposed system may be utilized during endoscopic surgery to present a BAM which carries important information for hemostasis.

1. Introduction

With the advancement of endoscopy, thoraco-laparoscopic surgery that enables minimally invasive operation is steadily becoming popular, replacing laparotomies and thoracotomies [1–7]. One of the long-standing problems with thoraco-laparoscopic surgery is the treatment for bleeding in the abdominal cavity [8–11]. Laparoscopic surgery is performed in a limited field of view and light source, so that the surgeon has to concentrate on the visual information in the center region of the device screen where he/she manipulates a surgical instrument [12,13]. Thus, a response to events such as bleeding occurring near the screen boundary tends to be delayed, leading to unnecessary

prolonged hemorrhage. Moreover, bleeding may obscure the surgical field view, decreasing visibility and complicating the surgical operation. Of course, bleeding itself causes damage to tissues, increasing the burden on patients, so that monitoring the extent of bleeding is extremely important for the judgment of whether or not an endoscopic surgery should be suspended [14,15].

In the field of wireless capsule endoscopy technique, there are several researches that develop systems for automatic bleeding detection from endoscopic images. For example, Jia and Meng [16] demonstrates an approach to bleeding detection based on segmentation of bleeding regions using deep learning. In addition, Caroppo et al. [17] proposed

* Corresponding author.

E-mail address: kkawa729@g.ecc.u-tokyo.ac.jp (K. Kawashima).

¹ Equally contribution in this paper.

a bleeding region detection method using transition learning that fuses the minimum redundancy maximum relevance method and different fusion rules.

Meanwhile, there are not many studies that utilize thoraco-laparoscopic images. Regarding bleed detection, Okamoto et al. [18] developed a method that uses the combination of RGB values and HSV values of images as input to a support vector machine to categorize the presence/absence of bleeding. Garcia-Martinez et al. [19] proposed a technique using RGB information from a single endoscopic image. By comparing and analyzing the ratio of red/blue and the ratio of red/green with the average pixel value throughout the operation as the threshold value, the bleeding area and the background area are separated to identify the existence of bleeding. The technique is particularly effective for large-scale hemorrhage. There are also researches on a framework for estimating the bleeding area in more detail, where a bounding box labeled by the surgeon is used for training data.

Among them, the estimation accuracy for a bleeding source and bleeding area has been improved by using spatio-temporal information of the site obtained from time-series image data [20]. However, if the surgeon moves the camera during surgery, the position of the bleeding source may not be constant, and it may be difficult to apply this technique at such moments. Moreover, surrounding tissues may be constantly deformed by the surgical instrument. If information from an image at a single time point allows accurate estimation, it would greatly contribute to the development of a safer hemostasis support system.

It should be also noted that hemostasis may be appropriately performed by applying a certain concentrated pressure to the bleeding site, so that identifying a bleeding source point, rather than a region, enables more effective hemostasis, avoiding unnecessary damage to the peripheral tissues [21]. However, when given as a point information, the possibility is greater that the specified site is deviated from a true bleeding source; in such cases, it is necessary to immediately move to a next bleeding source candidate and resume hemostasis.

For this purpose, it would be more advantageous and informative to provide the bleeding source candidate as an alert map, which shows information on the intensity related with probability of being the bleeding source for each point in the region, rather than providing the candidate as a flat region.

When applying AI techniques such as deep learning to image processing, crucial part is to obtain images suitable for the purpose of a problem and their correct labels. In order to identify bleeding and estimate its source, a pair set of a bleeding image and its corresponding bleeding source location is required, but such pair is difficult to obtain from actual surgical images. The issue was how to acquire training data for which the bleeding starting point is accurately known. We might use animal organs to obtain bleeding data, but the cost is high and there is also an ethical problem from the viewpoint of the principles of the 3Rs (Replacement, Reduction and Refinement) when using animal organs [22].

To solve these problems, we have developed a platform for bleeding source estimation which utilizes a newly created device, made up of silicone and agar, that can imitate bleeding behavior of a living organ. As we can arbitrarily position a bleeding source on the mimicking organ, it is easy to generate training data which contain clear correspondence between bleeding sources and subsequent bleeding images. From these data, we create a so-called bleeding alert map (BAM) that gives information about the probability of each point of being a bleeding source.

To generate the BAM, Pix2Pix, one of the Image to Image translation methods, was used for validation along with the generation of the alert map. Pix2Pix, which was proposed by Isola et al. [23], is a technology that realizes image-to-image translation such as generating an actual building image from its segmentation image and coloring an edge image. It is a kind of conditional GAN (Generative Adversarial Network). GAN is a network called a generative model that learns training data and generates new data similar to them. GAN consists

of two networks, a Generator model and Discriminator model. The Generator outputs a new composite image and the Discriminator model determines whether the image is a genuine one from the original data set or a fake one generated by the Generator. The Generator is trained so that the generated image may look like the genuine image to “fool” the Discriminator, while the Discriminator is trained so that it may correctly distinguish the genuine data and false data. At the end of training, the Generator may be able to produce an image similar to the training data.

We apply the trained Generator, which has been constructed by Pix2Pix using the bleeding image and source pairs from the mimicking device, to actual lung bleeding images as well as endoscopic images of organs obtained during actual clinical surgeries, and evaluate the performance of the Generator if it is capable of creating appropriate BAMs.

The contents of this paper are as follows: In Section 2, we describe our method for creating datasets with bleeding source information using a developed mimicking organ and how we use pix2pix to generate BAMs from the datasets. Section 3 describes the results of generated BAMs from bleeding images obtained from both the mimicking and actual organ *in vivo*. In Section 4, we discuss this technology’s potential future applications and improvements, also addressing potential limitations and proposed solutions. Finally, in Section 5, we conclude the paper.

2. Materials and methods

The overview of the proposed method is shown in Fig. 1. The proposed method consists of three phases. The first phase involves explaining a mimicking organ device capable of acquiring bleeding source information and creating a pair of Ground truth BAM information and bleeding images from the obtained information. In the second phase, a Generator, which generates a BAM using Pix2Pix, is trained based on the dataset from the first phase. Finally, the third phase involves the generation of a BAM by inputting actual bleeding images into the Generator trained in the second phase. The following subsection provides detailed descriptions of the mimicking device and the process of BAM generation.

2.1. Simulated vascular perfusion device

Fig. 2 shows a schematic diagram of the developed simulated blood vessel perfusion device (mimicking device). The device consists of a blood flow reproduction part and an organ part. The blood flow reproduction part comprises a peristaltic pump (MP-3N, Eyela Tokyo rikakikai Co., LTD., Tokyo, Japan), a 5 mm diameter connecting silicon tube (ARAM Corporation, Osaka, Japan), and a 3 mm diameter silicon tube embedded in the pseudo organ (AS ONE Corporation, Osaka, Japan), with perfusion performed at 0.3–0.5 mm/s. The simulated blood used was an aqueous solution of glycerin (Wakenyaku CO., LTD., Kyoto, Japan) (75% v/v) colored with acrylic paint. The concentration of glycerin was adjusted to be close to the spread of blood *in vivo*. The organ part includes a silicon base that imitates the surface of an organ and a coating layer on the surface made of 3% agar (Hayashi Pure Chemical IND., LTD., Japan), between which a silicon tube “blood vessel” is embedded. “Bleeding” was caused by puncturing the surface of the silicone tube with an 18G needle. Movie 1 shows a video of simulated bleeding for the device.

2.2. Preparation of training and validation image sets using the mimicking device

Images were taken with a handheld USB microscope and captured in a 1280 × 720 RGB, MPEG4 format video (20 fps). Leica CLS 150X (Leica Microsystems, Wetzlar, Germany) was employed as the light source, and the surroundings were covered with a blackout curtain at

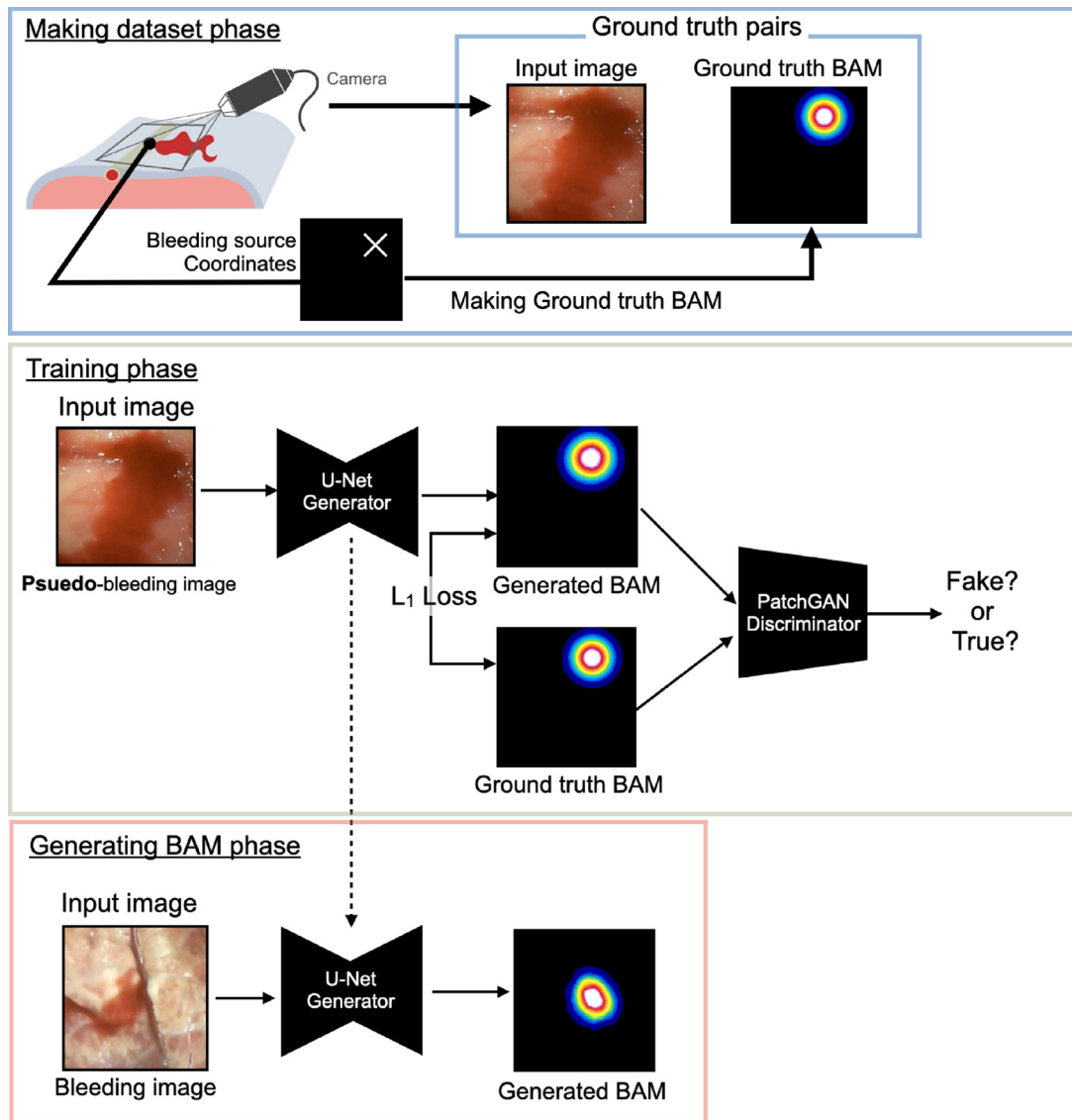


Fig. 1. Overview of making datasets phase and generating BAMs phase using Pix2Pix. Generator generates a BAM from RGB image input obtained from the mimicking device, and Discriminator determines the BAM is fake or true. Generator and Discriminator are optimized through hostile learning by using the BAMs created by the Generator and the ground truth BAMs. In the generating BAM phase, the BAM can be generated with inputs such as bleeding images from real organs. The BAMs are displayed in pseudo-color.

the time of imaging to reproduce the environment similar to that of an abdominal cavity.

In one experiment, the bleeding source position coordinate information and a total of 4 frames (one frame at the start of bleeding, one last frame when the image became stationary, 2 random frames in between the two frames) were collected. For each frame, 7 random rotations, enlargements and reductions, inversions were performed as data augmentation. The size of training/test images is 256×256 RGB, and a total of 3535 images were prepared to be used as training data. For test data, 200 pairs of input images and the ground truth BAMs were used, obtained from a different pattern of the bleeding mimicking device than that used for training. Additionally, to examine the changes in the BAM intensity at the bleeding source over time, ten series of video data were utilized for validation.

2.3. Acquisition of simulated bleeding images from a porcine lung by using two types of camera devices

Simulated blood was circulated to the intratissue vein of an excised porcine lung (10-months-old female, Shibaura organ, Tokyo, Japan) to

investigate whether the developed method is applicable to images from a blood vessel running on the actual organ surface. A total of 10 images were obtained using a handheld microscope. Separate experiments were performed with the KARL STORZ Image1 D3-Link camera system and TIPCAM1 telescope (30 fps, 1920×1080 RGB, KARL STORZ SE & Co. KG, Tuttlingen, Germany) as an image capturing device to collect another 10 images.

2.4. Acquisition of real bleeding images from laparotomy and thoracoscopy *in vivo*

We also collected actual bleeding images during laparotomy and endoscopic surgeries on living organs.

For the laparotomy images, we employed the video data from laparotomy operation on a porcine (Zenno-premium-pig, 2.5-months-old male, KAC Co., Ltd., Kyoto, Japan). The video data was obtained for verification on hemostasis [24,25]. All procedures and protocols were approved by the Animal Care and Use Committee of the National Cancer Center (authorization number: K19-007). The images were obtained using SONY FDR-AX55 (30 fps, 1920×1080 RGB, Sony

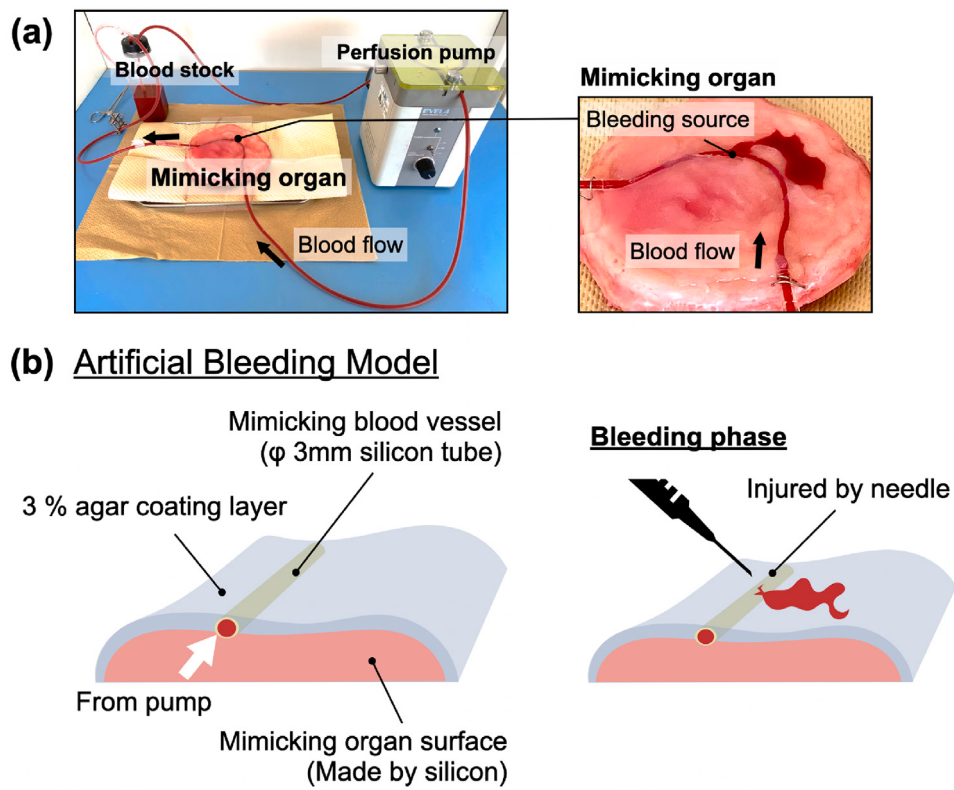


Fig. 2. Schematics of the simulated vascular perfusion device. (a): Overview of the device. Major components are a mimicking organ, a bloodstock container, and a circulation device. The right side figure shows a magnified view of the mimicking organ part when simulated bleeding is occurring. (b): Details of the mimicking organ. The mimicking organ consists of a colored silicon part that imitates the surface of an organ with a 3% agar layer that reproduces the epithelial feeling of an organ surface, and a silicon tube that imitates a blood vessel installed between the agar and silicon. Bleeding is initiated by puncturing the tube with a needle. (For interpretation of the references to color in this figure legend, the reader is referred to the web version of this article.)

Corporation, Tokyo, Japan). The organs to be imaged were a stomach, small intestine, and spleen, where bleeding was caused by surgical scissors, and the images were captured immediately after bleeding had started.

For the endoscopic surgery images, we employed the video data from a thoracoscopic operation on another porcine (LW species, female, 4-months-old female, Science Bleeding Co., Ltd., Chiba, Japan). The data was also obtained during the operational check of a surgical robot, where the research was approved by the Animal Research Committee of Tokyo Medical and Dental University (authorization number: A2020-061 A). Images were acquired using the KARL STORZ IMAGE1S camera system and 3D TIPCAM1 SPIES video telescope (60 fps, 1920 × 1080 RGB). The organ to be imaged was a lung. In this case study, there is no information on the bleeding source, because the images were from an actual surgery removing one of the lungs, where the bleeding source location was set as a rectangular region and labeled by surgeons and veterinarians.

2.5. Ground truth BAMs for training

The coordinates of the bleeding source can be easily obtained because it is possible to puncture the blood vessels of the mimicking organ with a needle at an arbitrary position here. The ground truth BAMs were defined from that information as a two-dimensional normal distribution centered on the bleeding source with a maximum value equal to 1:

$$f(\hat{x}, \mu, \Sigma) = \exp\left(-\frac{1}{2}(\hat{x} - \mu)^T \Sigma^{-1}(\hat{x} - \mu)\right) \quad (1)$$

where μ is the known coordinate point of the bleeding source, and Σ is the covariance matrix. In other words, the BAM intensity attenuates

with distance from the bleeding source. In this study, σ was chosen as $\sigma^2 I$, where I is a 2×2 identity matrix, and the parameter σ was determined so that the circular region of the distribution with intensity larger than 0.1 may cover approximately 5 times the diameter of the silicon tube blood vessel. In particular, the diameter is 25 mm as the real distance.

2.6. Construction of a BAM generator using Pix2Pix

Pix2Pix [23] was applied to construct a BAM Generator. The bleeding images used for input and the ground truth BAMs were originally $1280 \times 720 \times 3$ images, which then were scaled, rotated, and horizontally and vertically shifted, to be converted into cropped $256 \times 256 \times 3$ images for training input, with its details shown in the middle row of Fig. 1. First, we define G as a Generator that translates bleeding images into BAMs. U-Net [26] was used for the architecture of the Generator network. The encoder block includes a convolutional layer, a batch normalization layer, and a Leaky ReLU layer. In the encoder block, convolution was performed with 4×4 kernel and stride 2. The α value for the Leaky ReLU was set to 0.2. Tanh was used as the activation function for outputting the final output image. The decoder block consists of a transposed convolutional layer, a dropout layer, and a ReLU layer. The encoder and decoder blocks were connected by skip connections. The dropout rate for the dropout layer was set to 0.5. Also, we also defined D as a Discriminator, which distinguishes the generated image by the Generator and the ground truth BAM. Patch GAN was employed for the Discriminator network architecture. Each block consists of a convolutional layer, a batch normalization layer, and a Leaky ReLU layer ($\alpha = 0.2$). Patch GAN determines whether the effective receptive field is genuine or fake, with its patch size set to

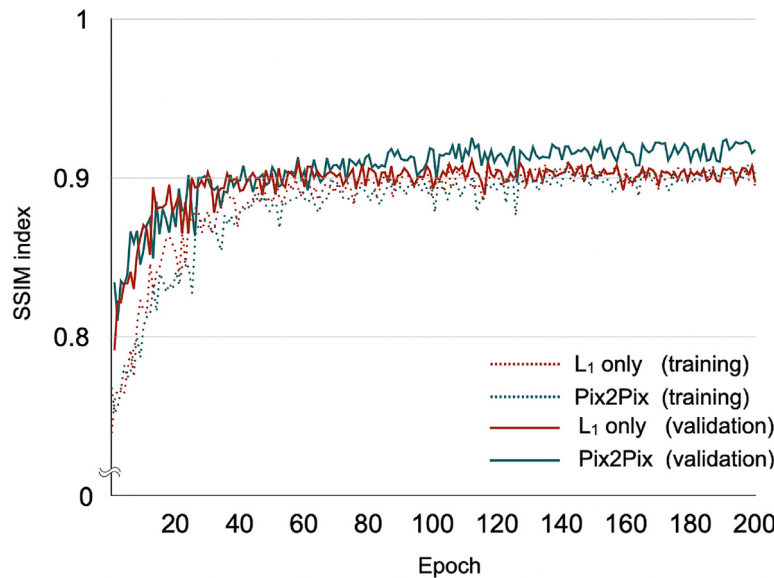


Fig. 3. The average of validation and training SSIM index in each epoch. Red and Green line indicates the case where L_1 only and Pix2Pix, respectively.

70 × 70 in this study. The architecture of the Pix2Pix model used for BAM generation in this study is shown in Supplementary Fig. 1.

The hostile loss functions of the networks are defined as follows.

$$\begin{aligned} \mathcal{L}_{cGAN}(G, D) = & \mathbb{E}_{x,y}[\log D(x, y)] + \\ & \mathbb{E}_{x,z}[\log(1 - D(x, G(x, z)))] \end{aligned} \quad (2)$$

$$\mathcal{L}_{L1}(G) = \mathbb{E}_{x,y,z} [\|y - G(x, z)\|_1]. \quad (3)$$

Therefore, the final objective is

$$G^* = \arg \min_G \max_D \mathcal{L}_{cGAN}(G, D) + \lambda \mathcal{L}_{L1}(G), \quad (4)$$

where the Discriminator D learns to maximize \mathcal{L} , and the Generator G learns to minimize \mathcal{L} . The Generator also considers the following L_1 loss so as not to generate an extreme image ignoring the dataset images. In this method, λ was set to 100. The results of learning with L_1 loss only (L_1 only) were compared with the Pix2Pix to verify the effectiveness of the Discriminator.

The neural network weights were initialized as a normal distribution with a mean of 1 and a standard deviation of 0.02, while the bias term was initialized to 0. Examples of an input image, Ground truth BAMs, generated BAMs, and the outputs derived from the Discriminator are shown in Supplementary Fig. 2. Adam optimizer with hyperparameters $\beta_1 = 0.5$ and $\beta_2 = 0.999$ was applied in the training. For the U-Net Generator, the networks were trained through 100 epochs with the learning rate 0.0002. The calculations were implemented on MATLAB 2021a (Mathworks, MA, USA) and it took 60 h for 200 epochs with Nvidia RTX2080 Ti.

For validation, three new image datasets, each consisting of 50 mimetic hemorrhage scene were used for evaluation, and the number of epochs used for evaluation was determined from the average. To evaluate the validation data, the structural similarity (SSIM) index [27] was used to determine the similarity between the created BAM images and the pre-defined ground truth BAM images (Fig. 3). Another 200 imitation image data were employed for the test data. Furthermore, in order to evaluate the generalization performance and verify the adaptability of the Generator trained with the mimic organ to the bleeding images from actual living organs, a total of 40 image sets using the actual excised organ as well as intraoperative images acquired under different conditions were utilized.

By using the Generator G with the learned parameters, BAMs were generated for the test data obtained from the simulated organ and for

other bleeding images from the actual organs. The final output BAMs are obtained as 256 × 256 RGB images converted to 8-bit grayscale images. The running time for creating the BAM was 0.098 s.

2.7. Image analysis and statistics

For the evaluation of the generated BAMs, the intensity value of the BAM at the actual bleeding source is calculated. The threshold value was set to 0.1, and the generation of the BAM was considered as successful when the intensity was larger than the threshold. Two kinds of evaluations were performed regarding the generation of the alert map. One is the evaluation of the judgment accuracy of bleeding state. The other is the evaluation of the extent to which the area of the generated alert map overlaps with that of the BAM generated from the ground truth or the bounding circle specified by humans, and how much of the areas do not overlap. As for the accuracy of the bleeding position estimation, the threshold of 0.1 was employed to determine if a bleeding source exists. If the source actually existed, it was judged that an alert map covering the bleeding position was successfully generated.

In order to verify the performance of the proposed method, the accuracy rate, precision rate, and recall rate are introduced as follows.

$$\text{accuracy rate} = \frac{TP + TN}{TP + TN + FP + FN}, \quad (5)$$

$$\text{precision rate} = \frac{TP}{TP + FP}, \quad (6)$$

$$\text{recall rate} = \frac{TP}{TP + FN}, \quad (7)$$

$$\text{F1 score} = \frac{2 \times \text{recall rate} \times \text{precision rate}}{\text{recall rate} + \text{precision rate}}, \quad (8)$$

where true positive is denoted as TP , false positive as FP , true negative as TN , and false negative as FN .

To generate the ROC (Receiver Operating Characteristic) curve, the true positive rate and the false positive rate were calculated as follows:

$$\text{true positive rate} = \frac{TP}{TP + FN}, \quad (9)$$

$$\text{false positive rate} = \frac{FP}{TN + FP}, \quad (10)$$

Alert Map evaluation

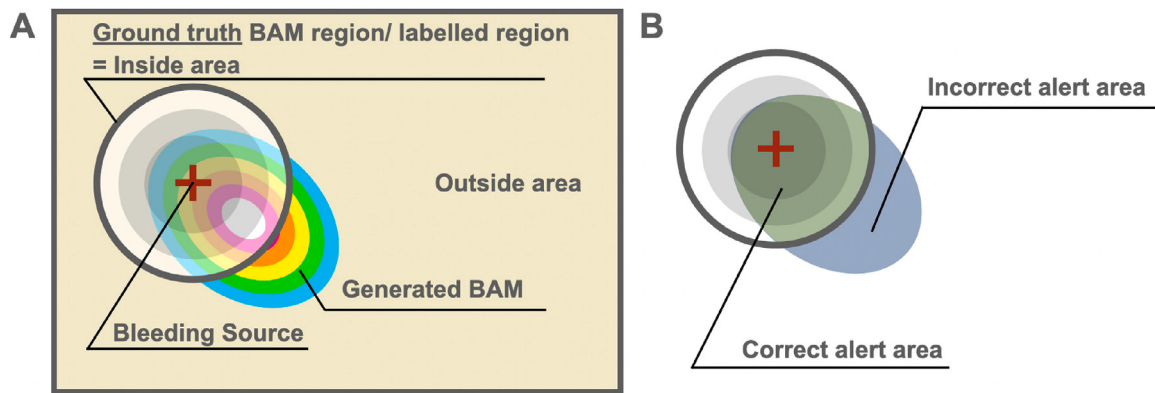


Fig. 4. Overview of the CAR and ICAR evaluations. The CAR indicates the ratio of generated BAMs to areas of ground truth BAMs above a threshold or areas labeled by humans; the ICAR indicates the ratio of BAMs present outside the correct region.

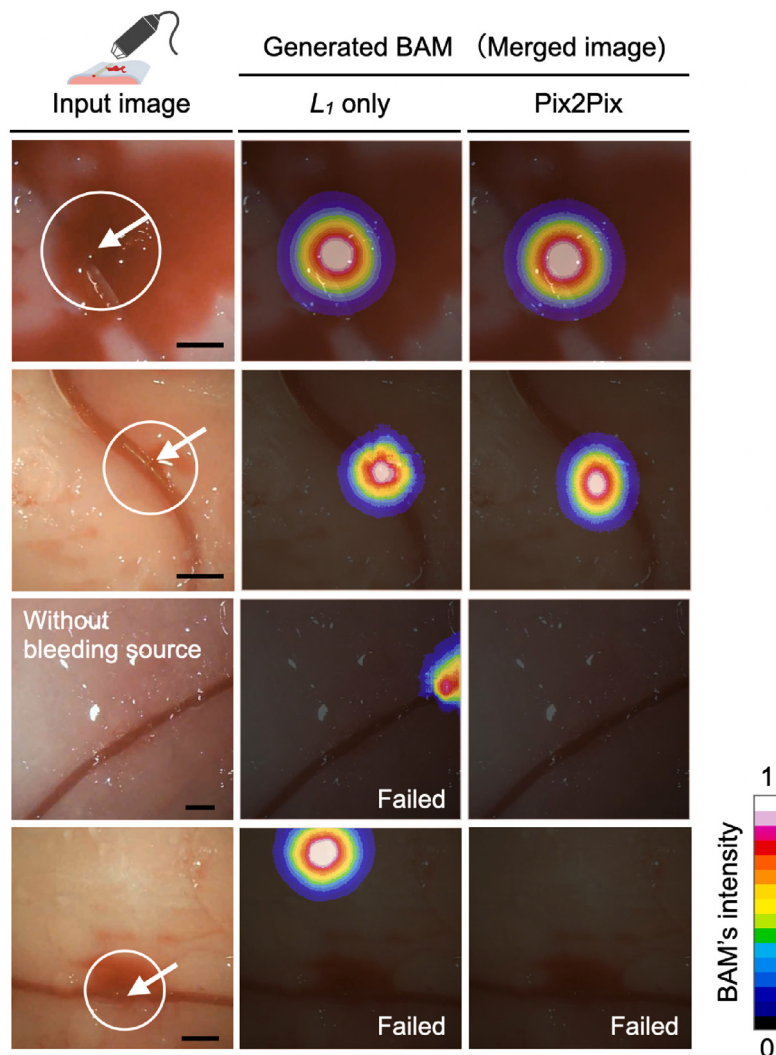


Fig. 5. BAM generation from test data using L_1 only and Pix2Pix. The left side image is the actual input image, and the middle image is the BAM created by L_1 only method, and the right side image is created by Pix2Pix. The white circular region indicates where the actual bleeding source was labeled as the ground truth. The intensity of the BAM follows the color bar at the bottom center (scale bar= 5 mm). (For interpretation of the references to color in this figure legend, the reader is referred to the web version of this article.)

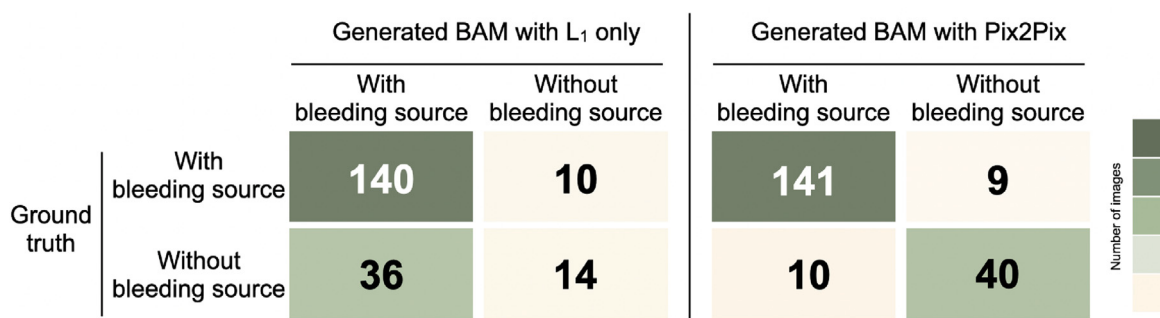


Fig. 6. Accuracy of the bleeding source identification by the BAM. The accuracy is shown as a confusion matrix that summarizes the evaluation result for the 200 test data using L_1 only and Pix2Pix. The color bar shows the number of elements. (For interpretation of the references to color in this figure legend, the reader is referred to the web version of this article.)

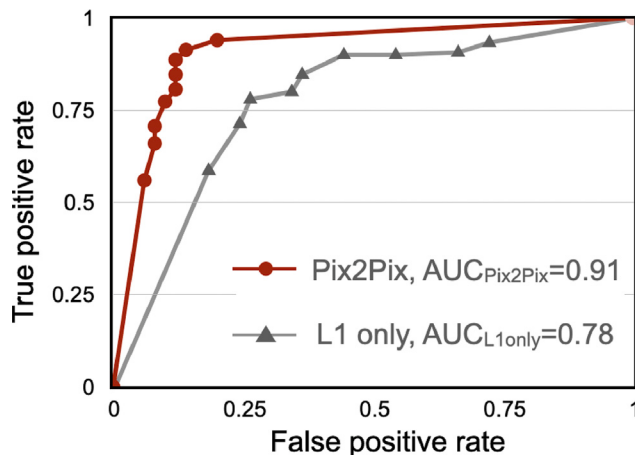


Fig. 7. The results of ROC curve using Pix2Pix and L_1 only.

The ROC curve was generated by changing the display threshold of the BAMs in increments of 0.1 from 0 to 1.

The CAR (correct alert rate) and ICAR (incorrect alert rate) are indicators similar to the IoU in the object recognition area, but here we use the different names to prevent confusion and show that they are specifically defined for alert maps (Fig. 4). With the region inside the ground truth alert map (intensity ≥ 0.1) or the bounding circle labeled by humans defined as *IR* (inside region), the region outside it defined as *OR* (outside region), and the number of pixels whose BAM intensity is ≥ 0.1 as *BAMR* (BAM region), CAR and ICAR are obtained as

$$\text{CAR} = \frac{\text{pixel}(IR \cap BAMR)}{\text{pixel}(IR)} * 100 \quad (11)$$

$$\text{ICAR} = \frac{\text{pixel}(OR \cap BAMR)}{\text{pixel}(OR)} * 100. \quad (12)$$

3. Results

3.1. Generation of BAMs for the test data from the mimicking device

Fig. 5 shows some of the test images used for the input to the Generator and the resulting BAMs. Fig. 6 shows the identification result of with-bleeding and without-bleeding sources using L_1 only and Pix2Pix on 200 test data. With the group of L_1 only, there are many cases of misrecognition where non-bleeding regions were often recognized as bleeding regions, with the accuracy rate being 77.0%, while the accuracy was improved to 90.5% for the BAM generation using Pix2pix. The recall rates were about the same (93.3% and 94.0%) for both cases. The precision rate was 79.5% for L_1 only, while it was higher at 93.4% for Pix2Pix. The F1 score was 0.94 when using Pix2Pix,

Table 1
The results of CAR and ICAR value in mimicking device.

Methods	CAR (%)	ICAR (%)
L_1 only	55.3	0.3
pix2pix	60.9*	0.4

n = 200.

*p value < 0.05.

and 0.85 with L_1 only. Additionally, a ROC curve was generated from the false positive rate/true positive rate of the generated BAM when the display threshold of BAM was varied in steps of 0.1 from 0 to 1, and an evaluation of AUC (Area Under the Curve) was conducted as well. The result is shown in Fig. 7. The AUC of the generated BAM using Pix2Pix was 0.91, whereas it was 0.78 in the case of L_1 only. This result suggests the effectiveness of the Discriminator in BAM generation.

Table 1 shows the CAR and ICAR results of the bleeding map generation areas. The CAR values increased significantly compared to the case of L_1 only, and the average was about 55.3% in the case of L_1 only, whereas it was about 60.9% in the case of Pix2Pix. No significant difference was found for the ICAR values.

Images at the early stages of bleeding also yield low intensities values. To account for these poor performances, we investigated how the intensities of BAMs at the bleeding sources change depending on the elapsed time from the start of bleeding. Fig. 8 shows the intensity values created from the start and spread of bleeding for 10 cases of video data. The intensities tend to be lower in the initial part.

3.2. Generation of BAMs from the porcine lung images obtained with the handheld camera ex vivo

Using the Generator constructed from the data for the mimicking device, we generated BAMs from the actual lung bleeding images. The imaging condition was the same as that for the mimicking device. Examples of the bleeding images and created BAMs are shown in Fig. 9. Even with the use of the commodity camera, it was mostly possible to generate correct BAMs. The CAR values were both about 80% (81% and 81.4% respectively). In both cases using L_1 only and Pix2Pix methods, the judgment was successful 9 out of 10 cases. In the one unsuccessful example, there was a bleeding source outside the area, but an alert map was generated within the imaging region.

3.3. Generation of BAMs from the porcine lung endoscopic images ex vivo

For similar excised organs, we also verified the results for the images obtained by a clinical endoscope which is different from the imaging device used for training. Additional difference from the images used for training is in that the images are from actual organs and they are obtained through an endoscope. The generated BAM image is shown in Fig. 10. The judgment accuracy in the case of L_1 only

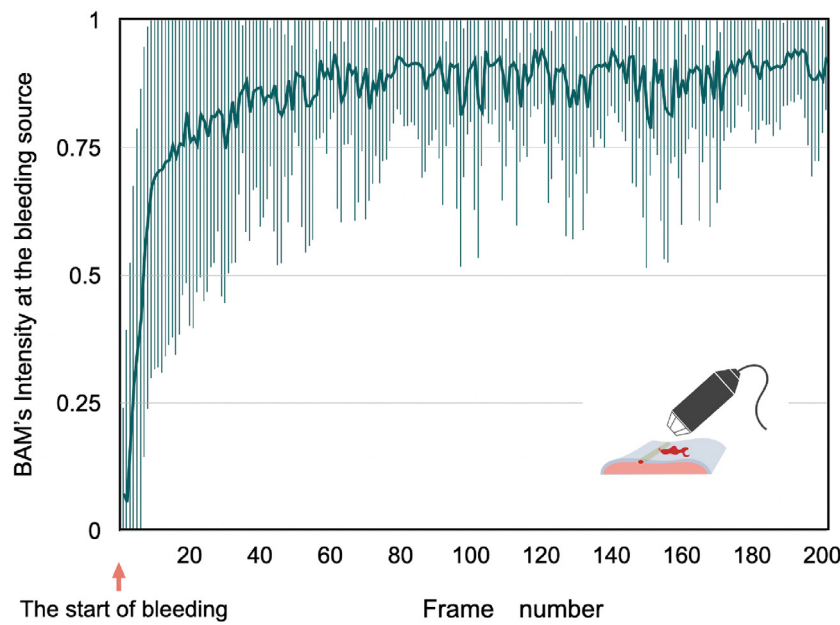


Fig. 8. Time variation in the intensity of the BAM at the bleeding source from the onset of bleeding using Pix2Pix. BAMs are generated for all video images from the start of bleeding to the 200th frame, which were acquired using the mimicking device. The time transition of the intensity of the BAM at the actual bleeding source is shown ($n = 10$, error bar: the maximum and minimum intensity).

Table 2

The results of CAR and ICAR value in ex vivo and in vivo samples.

Methods	CAR (%)			
	Excised lung + USB camera ($n = 10$)	Excised lung + Endoscope ($n = 10$)	Laparotomy ($n = 10$)	Thoracoscopic surgery ($n = 10$)
L_1 only	81.0	9.1	56.6	34.1
pix2pix	81.4	58.9*	63.6	71.0*
ICAR (%)				
Methods	Excised lung + USB camera	Excised lung + Endoscope	Laparotomy	Thoracoscopic surgery
L_1 only	5.8	5.4	7.7	8.4
pix2pix	3.6	4.3	9.2	12.2

* p value < 0.05 compared to each group.

was considerably deteriorated, with successful judgment being only 4 cases out of 10. On the other hand, in the case of Pix2Pix, the judgment was successful in 8 cases out of 10. The CAR was as low as 9.1% for L_1 only, while it was 58.9% for Pix2Pix. The ICAR values were 5.4% and 4.3% respectively. In particular, with Pix2Pix, a BAM was successfully created immediately after bleeding started, where the amount of bleeding was still very small.

3.4. Generation of BAMs from the surgical images using porcine organs in vivo

We made further verification of the generation accuracy for the images obtained from actual organs of a living pig instead of excised organs. Here, the verification was performed by using the camera images (Fig. 10) during laparotomy and the endoscopic images (Fig. 11) during thoracoscopic surgery.

In open surgery (Fig. 11), bleeding point information is available because the surgeon actually incised the organ to cause bleeding. In addition, the bleeding area was labeled by humans. The estimation of the bleeding position was successful in 8 out of 10 cases for both L_1 only and Pix2Pix. The CAR values using L_1 only and Pix2Pix were 56.6% and 63.6%, and the ICAR values were 7.7% and 9.2%, respectively.

Furthermore, we verified the accuracy of BAM generation from images during endoscopic surgery. Since it is difficult to obtain bleeding

source point information in this example, CAR and ICAR were verified in terms of their meaning based on the labeling information. The CAR value was as small as 34.1% when L_1 only was used, whereas it was 71.0% when the Discriminator was used, showing the significant increase in the accuracy of alert map generation. As for ICAR, the values using L_1 only and Pix2Pix were 8.4% and 12.2% respectively; the value for Pix2Pix is slightly higher, but there was no significant difference. When there was no bleeding, the generated BAM did not give any areas with bleeding source probability. Furthermore, in one case where blood is present but hemostasis is already applied and there is no bleeding, the generated BAM presented no bleeding source.

For the images from the thoracoscopic surgeries shown in Fig. 12. When there was no bleeding, the generated BAM did not give any areas with bleeding source probability. Furthermore, in one case where blood is present but hemostasis is already applied and there is no bleeding, the generated BAM presented no bleeding source.

4. Discussion

By using the BAM which is generated by the Generator constructed with the help of Pix2Pix, it has become possible to obtain probability information on a bleeding source on the endoscopic screen, while the conventional approaches are only capable of determining a segmented area where the bleeding source may exist. The accuracy at which a BAM could be correctly generated was 90.5%. Moreover, it has become

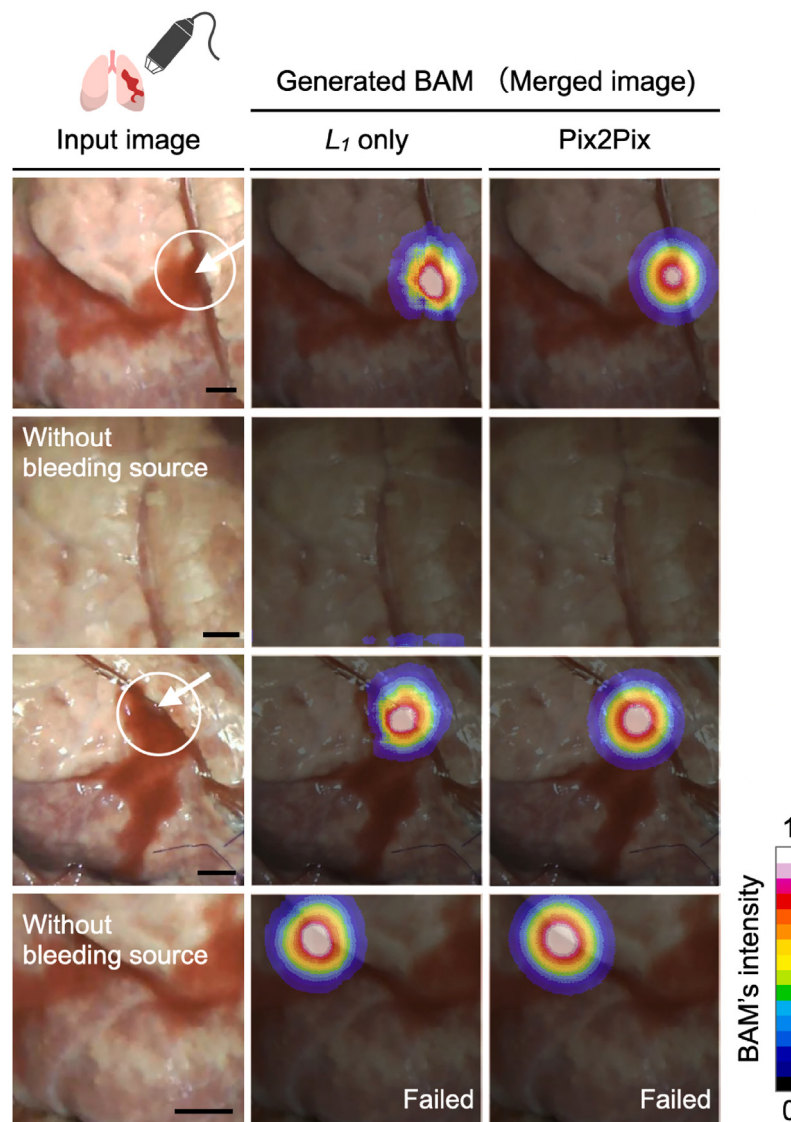


Fig. 9. BAM generation for the bleeding images from the excised porcine lung (a handheld microscope) using L_1 only and Pix2Pixel. The images were acquired under the same imaging conditions as the mimicking device. Blood was pumped into a blood vessel cannulated into the lung, and bleeding was caused by making a hole in the vessel by a needle. The left column is the actual input image, the center column is the generated BAM, and the right column is the merged image. The arrows indicate the actual bleeding point. The white circular region indicates where the actual bleeding source was labeled as the ground truth. The intensity of the BAM is shown according to the color bar at the lower right (scale bar = 5 mm). (For interpretation of the references to color in this figure legend, the reader is referred to the web version of this article.)

possible to estimate a bleeding source location from a single endoscopic image alone.

Table 2 summarizes the CAR and ICAR values when real tissues were used. From this result, it was suggested that a robust method is realized with the help of the Discriminator that does not impair the accuracy of bleeding source position estimation even in different imaging environment, although the generated range covered by the alert map tends to be slightly wider.

However, there are several points to consider regarding the proposed method. One of the concerns concerns the design of the ground truth BAMs. The developed system displays the area with a bleeding source as an intensity map of 0–1 instead of presenting an estimated bleeding source as a coordinate point. The size of the BAM generated in this study was about 0.5 to 2.0 cm. Since the equipment used for hemostasis is generally larger than this size, it should be possible to put the equipment accurately at the location specified by the BAM with white color showing the highest intensity. However, further study is needed on the design of the ground truth BAMs to achieve BAM visualization for detecting more accurate bleeding source that can

withstand clinical use. In addition, when used by surgeons, the optimal BAM intensity display and display range should be further designed with an eye toward hemostatic accuracy and display preference.

The advantage of this proposed method is that does not require preparing learning datasets acquired with a medical endoscope *in vivo* or *ex vivo* from actual organs. Instead, by using the artificial organ system and a commodity USB camera, it was possible to prepare datasets for the training of a Generator capable of producing reliable BAMs. As a result, we obtained accurate information on the bleeding source location, which is difficult to acquire during surgery. The Generator was then applied to the actual organs' bleeding images obtained *ex vivo* and *in vivo* by thoracoscope and endoscope to generate BAMs, which successfully identified correct bleeding sources. These results suggest that it is possible to develop a method that may adapt to actual intraoperative images by using datasets obtained by the mimicking device, which is cost-effective and conforms to the principles of the 3Rs.

Examples of failed BAM generation include the cases immediately after the start of bleeding, the cases where the bleeding source is

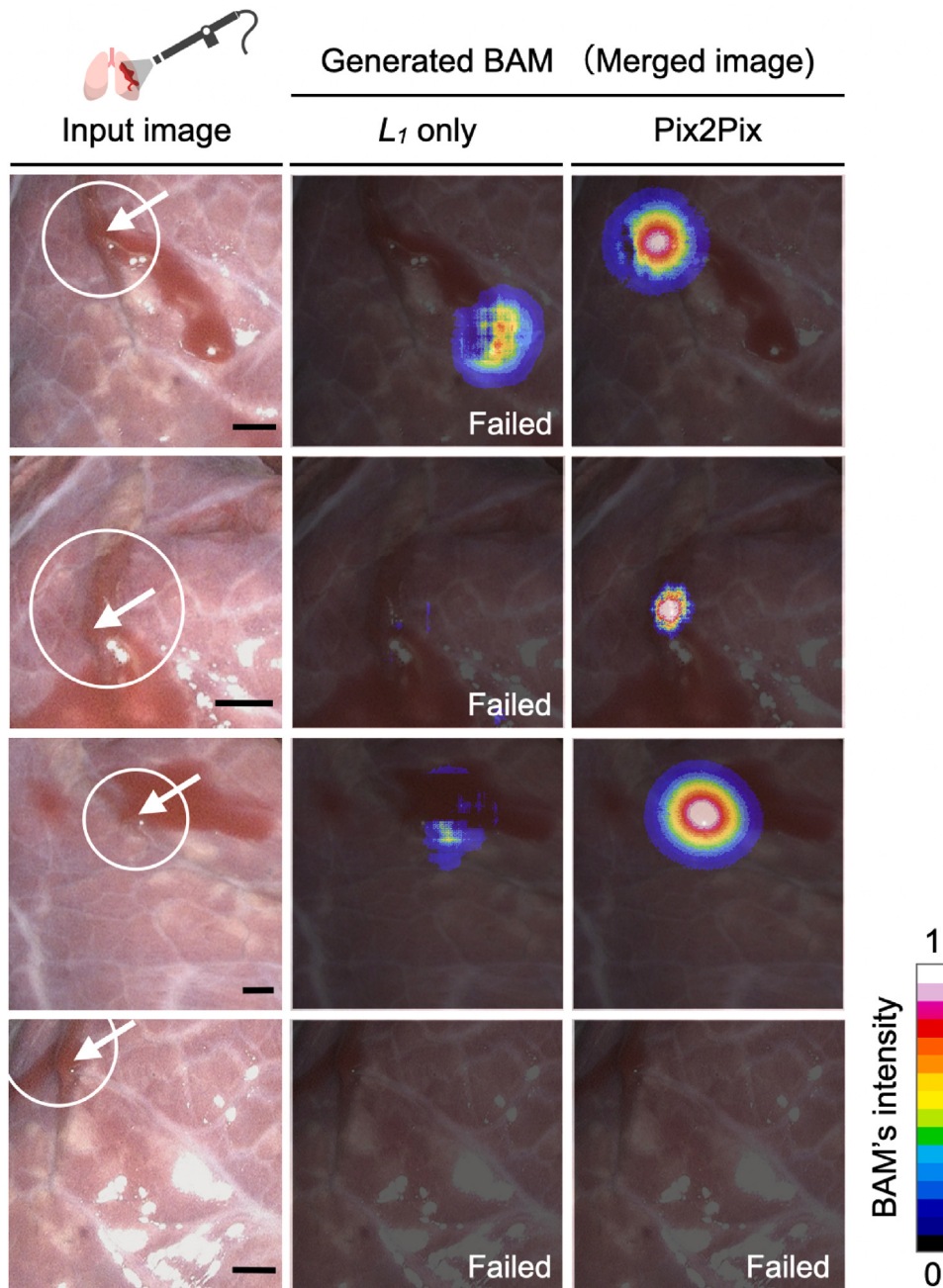


Fig. 10. BAM generation for the bleeding images from the excised porcine lung (a clinically used endoscope) using L_1 only and Pix2Pix. The left column is the actual input image, the middle column is the generated BAM using L_1 only, and the right column is the generated BAM using Pix2Pix. The arrows indicate the actual bleeding points. The white circular region indicates where the actual bleeding source was labeled as the ground truth. The intensity of the bleeding alert map at the bleeding point is shown according to the color bar in the lower right (Scale bar = 5 mm). (For interpretation of the references to color in this figure legend, the reader is referred to the web version of this article.)

outside the image, and the case where there is a groove structure blood flows in, which could not be expressed by the mimic device. In most of these cases, the data was obtained immediately after the initiation of bleeding. However, the intensity of the BAM at the bleeding source approached high intensity (>0.8) already after 50 frames (about 1.5 s) on average, which implies that hemostasis treatment could be initiated sufficiently early after the start of bleeding. In actual surgical situations, it has also been difficult to recognize the existence of bleeding before it has progressed to some extent by humans. So this method's capability of detecting bleeding and locating its source within about 1.5 s is considered a significant improvement. However, this is the case for

the 256×256 RGB image used to generate the BAM. In this day and age, endoscopes are becoming higher resolution, and endoscopic surgeries using 4 K and 8 K endoscopes are on the rise. In this case, the calculation time is expected to be longer, and it is necessary to consider algorithm acceleration to obtain real-time performance. In addition, when VR/AR is used for BAM information, there are issues such as whether rendering and information presentation should be 2D or 3D, and in such cases, speeding up the computation will be essential.

In this paper, Pix2Pix was employed as an image-to-image translation method for the verification of generated BAMs. BAMs, which have been shown to provide richer information than the conventional

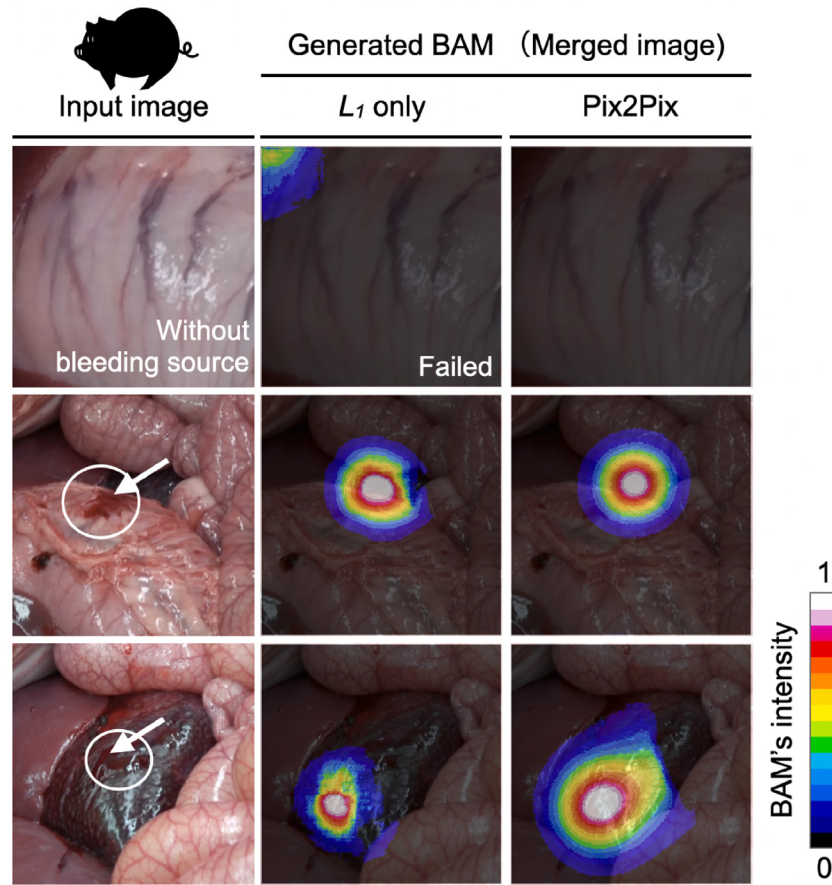


Fig. 11. BAM generation for the images obtained from actual pig laparotomy using L_1 only and Pix2Pix. The left column is the actual input image, the middle column is the generated BAM using L_1 only, and the right column is the generated BAM using Pix2Pix. The arrow indicates the actual bleeding source. The white circular region indicates where the actual bleeding source was labeled as the ground truth. The imaging system used was a SONY FDR-AX55. The input image to the Generator was a 256×256 RGB image, in which the organ part was cropped out of the original and reduced by 0.3 to 0.5 times so that the resulting image may be close to the scale of the images used for the training. The intensity of the BAM is shown according to the color bar at the bottom right. (For interpretation of the references to color in this figure legend, the reader is referred to the web version of this article.)

method, will be improved for higher accuracy and visibility by using a more state of the art image-to-image translation method in the future.

There are also several limitations of the proposed method. Furthermore, the method was developed by assuming bleeding occurs in blood vessels exposed on the tissue surface, because such vessels easily come into contact with surgical instruments. However, the current mimicking device does not assume a complicated shape and cannot provide depth information, so that bleeding that may occur at blood vessels running behind the organ or hidden in the back cannot be accounted for. As future work, a mimicking device incorporating a variety of features in the depth direction may be developed to further improve the performance of the system.

The proposed method also proposes a new provision method of bleeding state information called BAM. Since it differs from existing bleeding areas and labeling problems, it cannot be evaluated by direct image comparison. It is necessary to re-evaluate it in a clinical environment with scores such as improved hemostasis accuracy to clarify the effectiveness of the proposed method in the future.

A BAM an alert map that not only shows the location of a bleeding area but also has the expectation information of a bleeding source. Such information can be applied to Context-aware Augmented Reality in laparoscopic surgery [28,29], although issues such as real-time and clear visualization need to be considered. Furthermore, the ability to acquire detailed location information of a bleeding source would allow its application to hemostasis assistance under robot-assisted laparoscopic surgery as well as autonomous hemostasis.

5. Conclusion

In this paper, a simulated vascular perfusion system (mimicking device) was developed, which is capable of generating pair information of a post-bleeding image and a precise bleeding source location. Such information pairs were used as the input to Pix2Pix learning to construct a Generator that produces a “bleeding alert map (BAM)” presenting a location of the bleeding source as spatial distribution of intensity related to probability. By using the Generator created from the mimicking device data, BAMs for actual organs bleeding images were successfully generated. With the spread of thoraco-laparoscopic surgery, there is an increasing demand for an image processing system which is capable of recognizing intraoperative bleeding and estimating bleeding sources. This study has shown for the first time that the Generator created by using only the datasets from the mimicking device can reliably identify bleeding sources from actual bleeding organ images. This demonstrated that deep learning technology can be effectively applied to medical image processing where it is difficult to collect detailed learning datasets.

In the future, by adding more complexity to the mimicking device so that we may collect data for more difficult situations where bleeding comes from a deep layer of an organ which is outside the field view, we will develop a more advanced system which can accommodate such difficult circumstances. Furthermore, a safer hemostasis support system will be completed by combining this method with an estimation technique that uses time-series information.

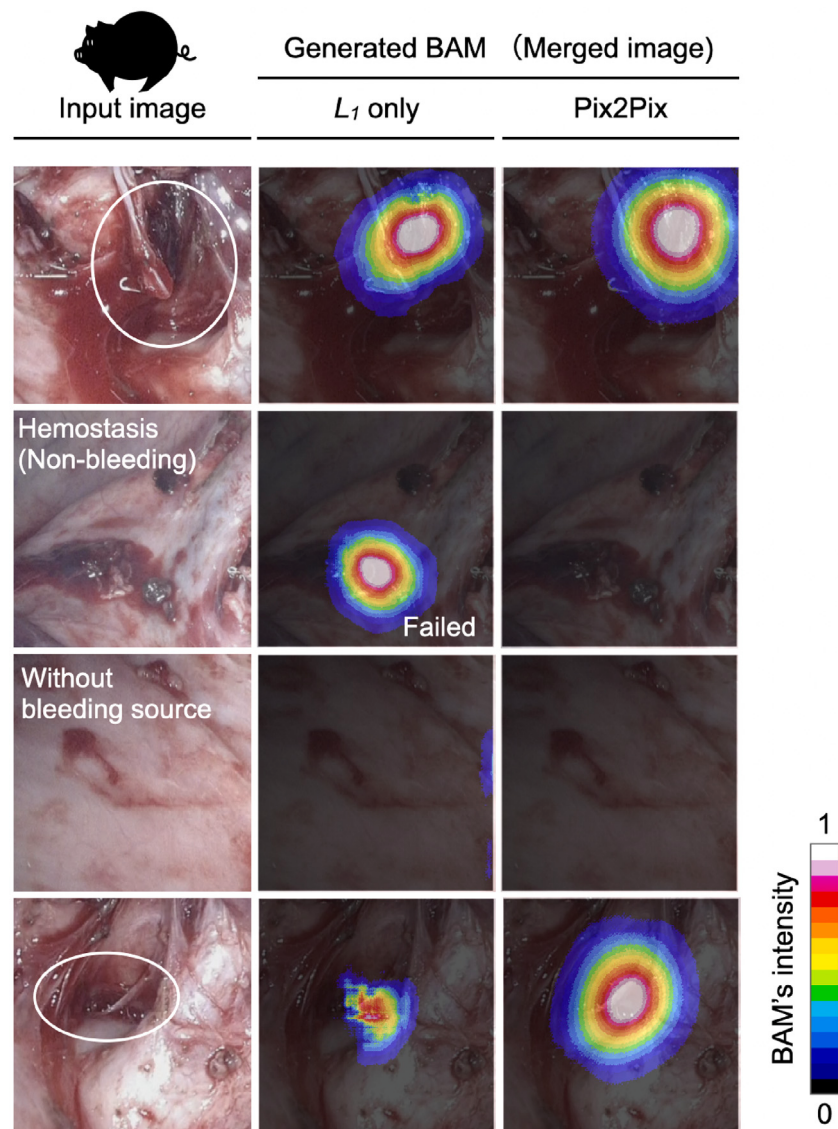


Fig. 12. BAM generation for the images obtained from actual one-lungectomy using a thoracoscope. The left column is the actual input image, the middle column is the generated BAM using L_1 only, and the right column is the generated BAM using Pix2Pix. The white circular region indicates where the actual bleeding source was labeled as the ground truth. The intensity of the BAM is shown according to the color bar at the bottom right. (For interpretation of the references to color in this figure legend, the reader is referred to the web version of this article.)

CRediT authorship contribution statement

Maina Sogabe: Conceptualization, Methodology, Investigation, Data Curation, Resources, Software, Writing- Original draft preparation, Writing- Reviewing & Editing, Visualization, Funding acquisition. **Kaoru Ishikawa:** Investigation, Data Curation, Resources, Writing- Original draft preparation, Writing- Reviewing & Editing. **Toshihiro Takamatsu:** Data Curation, Resources. **Koh Takeuchi:** Software, Formal analysis. **Takahiro Kanno:** Data Curation, Writing- Reviewing & Editing. **Koji Fujimoto:** Data Curation, Formal analysis. **Tetsuro Miyazaki:** Data Curation, Writing- Reviewing & Editing. **Toshihiro Kawase:** Data Curation. **Toshihiko Sato:** Resources. **Kenji Kawashima:** Supervision, Project administration, Writing- Original draft preparation, Writing- Reviewing & Editing.

Declaration of competing interest

The authors declare the following financial interests/personal relationships which may be considered as potential competing interests: Kenji Kawashima reports was provided by The University of

Tokyo. Kenji Kawashima reports a relationship with Riverfield Inc. that includes: equity or stocks.

Data availability

Data will be made available on request.

Acknowledgments

M. Sogabe is grateful to Dr. H. Sogabe, Dr. S. Uchida and Dr. N. Ito for suggesting the topic covered in this paper and thanks Dr. H. Seki for editing and proofreading this paper. This work was supported in part by JSPS KAKENHI Grant Number 21K18074 (Japan).

Appendix A. Supplementary data

Supplementary material related to this article can be found online at <https://doi.org/10.1016/j.array.2023.100308>.

References

- [1] Bateman BG, Kolp LA, Mills S. Endoscopic versus laparotomy management of endometriomas. *Fertil Steril* 1994;62:690–5. [http://dx.doi.org/10.1016/S0015-0282\(16\)56989-1](http://dx.doi.org/10.1016/S0015-0282(16)56989-1).
- [2] Weatherford DA, Stephenson JE, Taylor SM, Blackhurst D. Thoracoscopy versus thoracotomy: Indications and advantages. *Am Surg* 1995;61:83–6.
- [3] Whitson BA, Groth SS, Duval SJ, Swanson SJ, Maddaus MA. Surgery for early-stage non-small cell lung cancer: A systematic review of the video-assisted thoracoscopic surgery versus thoracotomy approaches to lobectomy. *Ann Thorac Surg* 2008;86:2008–16. <http://dx.doi.org/10.1016/j.athoracsur.2008.07.009>, discussion 2016.
- [4] Medeiros LR, Rosa DD, Bozzetti MC, Fachel JM, Furness S, Garry R, et al. Laparoscopy versus laparotomy for benign ovarian tumour. *Cochrane Database Syst Rev* 2009;2:CD004751. <http://dx.doi.org/10.1002/14651858.CD004751.pub3>.
- [5] Galaal K, Donkers H, Bryant A, Lopes AD. Laparoscopy versus laparotomy for the management of early stage endometrial cancer. *Cochrane Database Syst Rev* 2012;9:CD006655. <http://dx.doi.org/10.1002/14651858.CD006655.pub3>.
- [6] Borrueto FA, Impellizzeri P, Montalvo AS, Antonuccio P, Santacaterina E, Scalfari G, et al. Thoracoscopy versus thoracotomy for esophageal atresia and tracheoesophageal fistula repair: Review of the literature and meta-analysis. *Eur J Pediatr Surg* 2012;22:415–9. <http://dx.doi.org/10.1055/s-0032-1329711>.
- [7] Gala RB, Margulies R, Steinberg A, Murphy M, Lukban J, Jeppson P, et al. Systematic review of robotic surgery in gynecology: Robotic techniques compared with laparoscopy and laparotomy. *J Minim Invasive Gynecol* 2014;21:353–61. <http://dx.doi.org/10.1016/j.jmig.2013.11.010>.
- [8] McGinnis DE, Strup SE, Gomella LG. Management of hemorrhage during laparoscopy. *J Endourol* 2000;14:915–20. <http://dx.doi.org/10.1089/end.2000.14.915>.
- [9] Sugi K, Sudoh M, Hirazawa K, Matsuda E, Kaneda Y. Intrathoracic bleeding during video-assisted thoracoscopic lobectomy and segmentectomy. *Kyobu Geka* 2003;56:928–31.
- [10] Martay K, Dembo G, Vater Y, Charpentier K, Levy A, Bakthavatsalam R, et al. Unexpected surgical difficulties leading to hemorrhage and gas embolus during laparoscopic donor nephrectomy: A case report. *Can J Anaesth* 2003;50:891–4. <http://dx.doi.org/10.1007/BF03018734>.
- [11] Rosevear HM, Montgomery JS, Roberts WW, Wolf JS. Characterization and management of postoperative hemorrhage following upper retroperitoneal laparoscopic surgery. *J Urol* 2006;176:1458–62. <http://dx.doi.org/10.1016/j.juro.2006.06.023>.
- [12] Vargas-Palacios A, Hulme C, Veale T, Downey CL. Systematic review of retraction devices for laparoscopic surgery. *Surg Innov* 2016;23:90–101. <http://dx.doi.org/10.1177/1553350615587991>.
- [13] Bolton WS, Aruparyail NK, Chauhan M, Kitchen WR, Gnanaraj KJN, Benton AM, et al. Gasless laparoscopic surgery for minimally invasive surgery in low-resource settings: Methods for evaluating surgical field of view and abdominal wall lift force. *Surg Innov* 2021;28:513–5. <http://dx.doi.org/10.1177/1553350620964331>.
- [14] Boni L, Benevento A, Dionigi G, Dionigi R. A new device for minor bleeding control and blunt dissection in minimally invasive surgery. *Surg Endosc* 2003;17:282–4. <http://dx.doi.org/10.1007/s00464-002-9038-9>.
- [15] Miyazawa M, Aikawa M, Okada K, Watanabe Y, Okamoto K, Koyama I. Laparoscopic liver resection using a monopolar soft-coagulation device to provide maximum intraoperative bleeding control for the treatment of hepatocellular carcinoma. *Surg Endosc* 2018;32:2157–8. <http://dx.doi.org/10.1007/s00464-017-5829-x>.
- [16] Jia X, Meng MQ. A deep convolutional neural network for bleeding detection in wireless capsule endoscopy images. In: *Biology and society annuaire international conference IEEE eng. Med.* 2016, p. 639–42. <http://dx.doi.org/10.1109/EMBC.2016.7590783>.
- [17] Caroppo A, Leone A, Siciliano P. Deep transfer learning approaches for bleeding detection in endoscopy images. *Comput Med Imaging Graph* 2021;88:101852. <http://dx.doi.org/10.1016/j.compmedimag.2020.101852>.
- [18] Okamoto T, Ohnishi T, Kawahira H, Dergachyava O, Jannin P, Haneishi H. Real-time identification of blood regions for hemostasis support in laparoscopic surgery. *Signal Image Video Process* 2019;13:405–12. <http://dx.doi.org/10.1007/s11760-018-1369-7>.
- [19] Garcia-Martinez A, Vicente-Samper JM, Sabater-Navarro JM. Automatic detection of surgical haemorrhage using computer vision. *Artif Intell Med* 2017;78:55–60. <http://dx.doi.org/10.1016/j.artmed.2017.06.002>.
- [20] Jiang J, Lu Y, Hua S. Using spatiotemporal hybrid features for detecting bleeding point in laparoscopic surgery. In: *ICGIP*, vol. 11720. 2020, 117200C. <http://dx.doi.org/10.1117/12.2589338>.
- [21] D'Ambra L, Berti S, Bonfante P, Bianchi C, Gianquinto D, Falco E. Hemostatic step-by-step procedure to control presacral bleeding during laparoscopic total mesorectal excision. *World J Surg* 2009;33:812–5. <http://dx.doi.org/10.1007/s00268-008-9846-8>.
- [22] Russell WMS, Burch RL. *The principles of humane experimental technique*. London: Methuen and Co. Ltd.; 1959.
- [23] Isola P, Zhu JY, Zhou T, Efros AA. Image-to-image translation with conditional adversarial networks. In: *Proceedings of the IEEE computability social conference comput. vis. pattern recognit.* 2018, p. 1125–34.
- [24] Nomura Y, Takamatsu T, Kawano H, Miyahara H, Okino A, Yoshida M, et al. Investigation of blood coagulation effect of nonthermal multigas plasma jet in Vitro and in Vivo. *J Surg Res* 2017;219:302–9. <http://dx.doi.org/10.1016/j.jss.2017.06.055>.
- [25] Kurosawa M, Takamatsu T, Kawano H, Hayashi Y, Miyahara H, Ota S, et al. Endoscopic hemostasis in porcine gastrointestinal tract using CO2 low-temperature plasma jet. *J Surg Res* 2019;234:334–42. <http://dx.doi.org/10.1016/j.jss.2018.09.068>.
- [26] Ronneberger O, Fischer P, Brox T. U-net: Convolutional networks for biomedical image segmentation. In: *Int. conf. med. image comput. comput. assist. interv.* 2015, p. 234–41. http://dx.doi.org/10.1007/978-3-319-24574-4_28.
- [27] Wang Z, Bovik AC, Sheikh HR, Simoncelli EP. Image quality assessment: From error visibility to structural similarity. *IEEE Trans Image Process* 2004;13:600–12. <http://dx.doi.org/10.1109/tip.2003.819861>.
- [28] Kersten-Oertel M, Jannin P, Collins DL. The state of the art of visualization in mixed reality image guided surgery. *Comput Med Imaging Graph* 2013;37(2):98–112. <http://dx.doi.org/10.1016/j.compmedimag.2013.01.009>.
- [29] Katic D, Wekerle AL, Görtler J, Spengler P, Bodenstedt S, Röhl S, et al. Context-aware Augmented Reality in laparoscopic surgery. *Comput Med Imaging Graph* 2013;37(2):174–82. <http://dx.doi.org/10.1016/j.compmedimag.2013.03.003>.